RIS-Enabled Transmitter Design for Joint Radar and Communication

Emanuele Grossi
Dept. of Electr. and Inform. Eng.
Univ. of Cassino and Southern Lazio
03043 Cassino, Italy
e.grossi@unicas.it

Marco Lops
Dept. of Electr. Eng. and Inform. Tech.
Univ. of Naples "Federico II"
80138 Naples, Italy
lops@unina.it

Luca Venturino
Dept. of Electr. and Inform. Eng.
Univ. of Cassino and Southern Lazio
03043 Cassino, Italy
l.venturino@unicas.it

2025 IEEE Radar Conference (RadarConf25) | 979-8-3315-4433-1/25/$31.00 ©2025 IEEE | DOI: 10.1109/RADARCONF2559087.2025.11205094

***Abstract*—Achieving efficient and cost-effective transmit beampattern control for integrated sensing and communication (ISAC) systems is a significant challenge. This paper addresses this by proposing a dual-function radar communication (DFRC) transmitter based on a reconfigurable intelligent surface (RIS) illuminated by a limited number of active sources. We formulate and solve the joint design of source waveforms and RIS phase shifts to match a desired space-frequency radiation pattern, and we evaluate the resulting ISAC system's performance in terms of radar detection probability and data transmission rate. Numerical results demonstrate the promising capabilities of this RIS-enabled transmitter for ISAC applications.**

***Index Terms*—Integrated sensing and communication (ISAC), dual-function radar communication (DFRC), reconfigurable intelligent surface (RIS), beampattern design, detection probability, data transmission rate.**

I. Introduction

The synthesis of a desired transmit beampattern, representing a specific amplitude (or power) distribution of far-field electromagnetic radiation in space and frequency, is a classical problem in digital array processing. This is particularly relevant in integrated sensing and communication (ISAC) systems, where a dual-function radar communication (DFRC) transmitter can shape the transmit beampattern to simultaneously monitor a region and serve a communication user [1]–[3]. Achieving the desired beampattern often necessitates large (or even massive) antenna arrays, and the implementation of fully digital arrays, where each antenna element is controlled by a dedicated radio frequency (RF) chain, can be impractical due to high cost and energy consumption [4]. While hybrid analog-digital arrays have been proposed [5], their scalability with the number of antennas remains limited by the power consumption of the analog network [6]. Reconfigurable intelligent surfaces (RISs) have recently emerged as a promising solution to address these challenges, offering energy-efficient techniques with low-cost hardware, as demonstrated in metasurface-based transmitters [7], RIS-aided antennas [6], and transmitter-type RISs [8]. RISs, whether passive or active, can be controlled and reconfigured almost in real time.

In this work, we address the design problem for a RIS-based DFRC transmitter, where a small number of active antennas, referred to as sources (each equipped with a dedicated RF chain), illuminate a passive RIS (composed of numerous low-cost and energy-efficient elements), which reflects or retransmits a phase-shifted version of the superimposed incident signals. This RIS-based transmit architecture, already introduced in [6], [9], offers several advantages, including scalability (as beam-steering is controlled by the passive RIS elements) and higher energy efficiency in its feeding mechanism compared to hybrid analog-digital arrays [6]. It finds potential applications in MIMO communication systems [6], radars [10]–[13], and DFRC systems [14]–[17]. The beampattern design for antenna array has been studied in the context of MIMO radars [18]–[22] and in DFRC systems [1], [23]–[25]. In these works, the the probing waveforms are designed to match a desired beampattern in a least-squares (LS) sense. For the considered RIS-based transmit architecture, this LS design has been investigated only in [26], [27] for narrowband systems (with a single source in [26]) and without waveform design.

Building upon preliminary results for a radar system [28], this work presents and formulates the DFRC transmitter design problem, where the waveforms emitted by the sources and the phase shifts introduced by the RIS are jointly optimized. Furthermore, we analyze the ISAC system's performance in terms of radar sensitivity (measured by the probability of detection for a fixed probability of false alarm) and communication throughput (measured by the supremum of the achievable data rates). Finally, we provide an example demonstrating the inherent tradeoff between these two functionalities. Importantly, despite utilizing significantly fewer active sources compared to fully digital MIMO systems, the RIS-based architecture shows promising performance in terms of both achievable detection probability and data transmission rate.

The remainder of the paper is organized as follows: Sec. II describes the considered RIS-based DFRC transmit and derives the signal model and beampattern. Sec. III presents the beampattern matching problem and provides a performance

The authors are also with Consorzio Nazionale Interuniversitario per le Telecomunicazioni (CNIT), 43124 Parma, Italy. The work of E. Grossi and M. Lops was supported by the European Union – Next-GenerationEU – National Recovery and Resilience Plan (NRRP) – Mssion 4 Component 2, Investment n. 1.3, Call 341 15-03-2022 (Project PE00000001, program "RESTART," CUP n. E63C22002040007). The work of L. Venturino was supported by the European Union – Next-GenerationEU – National Recovery and Resilience Plan (NRRP) – Mission 4 Component 2, Investment n. 1.1, Call PRIN 2022 D.D. 104 02-02-2022 (Project 202238BJ2R CIRCE, CUP n. H53D23000420006).

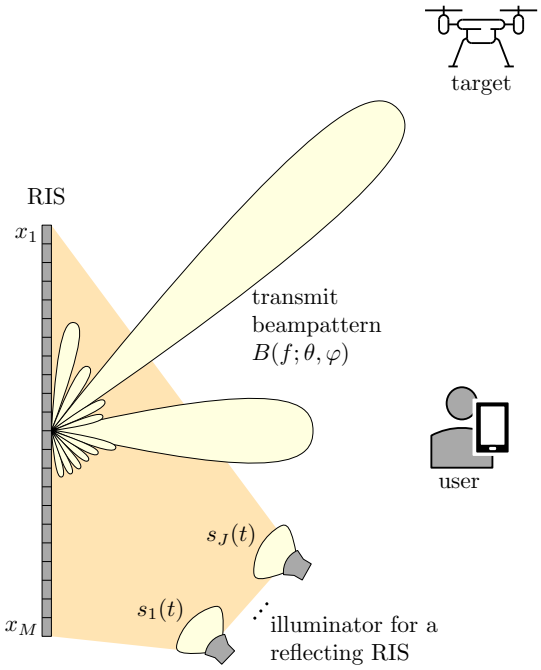

Figure 1. Considered DFRC transmit architecture, composed of an illuminator with J sources and a passive RIS with M elements used to form multiple beams for radar sensing and communication. The RIS can either be reflecting (as in this figure) or transmitting (in this case, the illuminator is placed behind the surface).

analysis. Sec. IV presents a numerical example to demonstrate the operating points and advantages of this ISAC system. Finally, concluding remarks are given in Sec. V.

II. System model

Consider the DFRC system illustrated in Fig. 1, where J sources illuminate a passive RIS with M elements to form multiple beams for radar sensing and communication. For a reflecting RIS, the illuminator is located on the same side as the target and the user. In contrast, for a transmitting RIS, it is situated on the opposite side (i.e., behind the RIS), as shown in Fig. 1. The lowpass signal emitted by the j-th source is given by $as_j(t)$, where a is a random variable with a unit mean square value, representing the communication symbol sent to the user by the transmitter, and $s_j(t)$ is the baseband radar-communication pulse, with its support contained within the interval $[0,T]$ and Fourier transform, $S_j(f)$, approximately zero outside the interval $[-W/2, W/2]$. The carrier frequency is f_c, and the channel linking source j, the i-th element of the RIS, and a point (r,θ,φ) in the far-field region is modeled as

$$H_{ij}(f;r,\theta,\varphi) = \frac{\mathrm{e}^{-2\pi \mathrm{i} f(r/c+\tau_i(\theta,\varphi))}}{\sqrt{4\pi r^2}}\Gamma_i(\theta,\varphi)x_i G_{ij}(f), \quad (1)$$

where i is the imaginary unit, $G_{ij}(f)$ represents the channel between source j and the i-th element of the RIS, x_i is a unit-modulus complex scalar representing the response of the i-th RIS element, $\Gamma_i(\theta,\varphi)$ is the amplitude beampattern of the i-th RIS element, $\sqrt{4\pi r^2}$ accounts for the free-space attenuation from the RIS to the observation point, and $r/c+\tau_i(\theta,\varphi)$ is the corresponding propagation delay, with c being the speed of light and $\tau_i(\theta,\varphi)$ the differential delay with respect to the center of gravity of the RIS.

The Fourier transform of the complex envelope of the signal observed at (r,θ,φ) is given by[1]

$$\begin{aligned} Y(f;r,\theta,\varphi) &= a\sum_{i=1}^{M}\sum_{j=1}^{J} H_{ij}(f+f_c;r,\theta,\varphi)S_j(f) \\ &= \frac{a}{\sqrt{4\pi r^2}}\mathrm{e}^{-2\pi\mathrm{i}(f+f_c)r/c} \\ &\quad \times \boldsymbol{v}^{\mathsf{H}}(f;\theta,\varphi)\,\mathrm{diag}(\boldsymbol{x})\boldsymbol{\Omega}(f;\theta,\varphi)\boldsymbol{\sigma}(f), \end{aligned} \quad (2)$$

where $\boldsymbol{v}(f;\theta,\varphi) = [\mathrm{e}^{2\pi\mathrm{i}(f+f_c)\tau_1(\theta,\varphi)} \ \dots \ \mathrm{e}^{2\pi\mathrm{i}(f+f_c)\tau_M(\theta,\varphi)}]^{\mathsf{T}}$, $(\cdot)^{\mathsf{T}}$ denoting transpose, is the steering vector in the direction (θ,φ) at frequency f, $(\cdot)^{\mathsf{H}}$ denotes conjugate transpose, $\boldsymbol{x} = [x_1 \ \cdots \ x_M]^{\mathsf{T}} \in \mathbb{C}^M$, $\mathrm{diag}(\boldsymbol{x})$ is a diagonal matrix with the elements of $\boldsymbol{x}$ on the main diagonal, $\boldsymbol{\Omega}(f;\theta,\varphi)$ the $M\times J$ complex matrix whose entry (i,j) is $\Omega_{ij}(f;\theta,\varphi) = G_{ij}(f+f_c)\Gamma_i(\theta,\varphi)$, and $\boldsymbol{\sigma}(f) = [S_1(f) \ \cdots \ S_J(f)]^{\mathsf{T}} \in \mathbb{C}^J$.

Given that the source signals are bandlimited, we can approximate $S_j(f) \approx \frac{1}{W}\sum_{n=1}^{N} s_j(n/W)\mathrm{e}^{-2\pi nf/W}$, where $N = \lfloor WT \rfloor$. Thus, by defining the n-th sample of the signal vector as $\boldsymbol{s}_n = [s_1(n/W) \ \cdots \ s_J(n/W)]^{\mathsf{T}} \in \mathbb{C}^J$, and the whole signal as $\boldsymbol{s} = [\boldsymbol{s}_1^{\mathsf{T}} \ \cdots \ \boldsymbol{s}_N^{\mathsf{T}}]^{\mathsf{T}} \in \mathbb{C}^{JN}$, we can approximate (2) as

$$\begin{aligned} Y(f;r,\theta,\varphi) &\approx a\sqrt{\frac{T}{4\pi r^2}}\mathrm{e}^{-2\pi\mathrm{i}(f+f_c)r/c} \\ &\quad \times \boldsymbol{v}^{\mathsf{H}}(f;\theta,\varphi)\,\mathrm{diag}(\boldsymbol{x})\boldsymbol{Q}(f;\theta,\varphi)\boldsymbol{s}, \end{aligned} \quad (3)$$

where[2]

$$\boldsymbol{e}(f) = \begin{bmatrix}\mathrm{e}^{-2\pi\mathrm{i}f/W} & \cdots & \mathrm{e}^{-2\pi\mathrm{i}Nf/W}\end{bmatrix}^{\mathsf{T}} \in \mathbb{C}^N \quad (4)$$

$$\boldsymbol{Q}(f;\theta,\varphi) = \frac{1}{W\sqrt{T}}\tilde{\boldsymbol{G}}(f;\theta,\varphi)\big(\boldsymbol{e}^{\mathsf{T}}(f)\otimes \boldsymbol{I}_J\big) \in \mathbb{C}^{M\times JN}, \quad (5)$$

and the (amplitude) beampattern is

$$\begin{aligned} B(f;\theta,\varphi) &\approx \sqrt{\frac{4\pi r^2}{T}\mathbb{E}\left[\left|Y(f;r,\theta,\varphi)\right|^2\right]} \\ &= \left|\boldsymbol{v}^{\mathsf{H}}(f;\theta,\varphi)\,\mathrm{diag}(\boldsymbol{x})\boldsymbol{Q}(f;\theta,\varphi)\boldsymbol{s}\right|, \end{aligned} \quad (6)$$

where $\mathbb{E}[\,\cdot\,]$ denotes statistical expectation.[3] This general model holds for both narrowband and broadband architectures; the operating regime (narrowband/broadband) depends on the RIS size, the source positions, and the signal bandwidth.

III. System design and Performance analysis

The DFRC transmitter forms a narrow beam across the frequency band allocated for radar and steers it to scan the monitored area for potential targets, whose position, response, and even presence are unknown. For communication, perfect

[1] Vectors and matrices are denoted by lowercase and uppercase boldface letters, respectively.

[2] $\boldsymbol{I}_J$ denotes the $J\times J$ identity matrix and $\otimes$ is the Kronecker product.

[3] Notice that $Y(f;r,\theta,\varphi)$ contains the communication symbol a, which is a random variable.

channel state information (CSI) is assumed at the transmitter, and a fixed beam is formed towards the user, utilizing the frequency band allocated for communication.

The resource to be allocated is thus the space-frequency distribution of the transmit power, defined by $B(f;\theta,\varphi)$. The objective is to design the source signals and the RIS phases such that the amplitude beampattern $B(f;\theta,\varphi)$ matches a desired amplitude beampattern, say $D(f;\theta,\varphi)$, in an LS sense. LS amplitude beampattern matching is a widely accepted design criterion in recent years (see, e.g., [21]). Discretizing the angular region $[-\pi/2,\pi/2]^2$ with L points, namely $\{(\theta_\ell,\varphi_\ell)\}_{\ell=1}^L$, and the frequency region $[-W/2,W/2]$ with K points, namely $\{f_k\}_{k=1}^K$, the beampattern matching problem can be formulated as:

$$\begin{aligned}\min_{\boldsymbol{s}\in\mathbb{C}^{JN},\boldsymbol{x}\in\mathbb{C}^M}\ & \sum_{k=1}^{K}\sum_{\ell=1}^{L} w_{k\ell}\big(D(f_k;\theta_\ell,\varphi_\ell)-B(f_k;\theta_\ell,\varphi_\ell)\big)^2,\\ \text{s.t. }& \frac{1}{N}\|\boldsymbol{s}\|^2\le P,\\ & |x_i|=1,\quad \forall i,\end{aligned} \tag{7}$$

where $\{w_{k\ell}\}_{k\ell}$ are given weights allowing for emphasis on different regions, $\|\cdot\|$ is the Euclidean norm, and P is the available power at the illuminator. This problem is quite complex, and we refer to [28]—which considered a pure radar system—for a suboptimal solution using the block-coordinate descent method (alternating minimization).[4]

Once the beampattern is designed, radar performance is evaluated by the probability of target detection for a fixed false alarm probability. The receiver is colocated with the RIS-based transmit architecture and is equipped with an antenna with gain $G_{\text{rx,r}}(\theta,\varphi)$. If a target is present at (r_t,θ_t,φ_t), the Fourier transform of the complex envelope of the backscattered signal at the radar receiver (colocated with the DFRC transmitter) is:

$$\begin{aligned}Z_r(f;r_t,\theta_t,\varphi_t) = Y(f;r_t,\theta_t,\varphi_t)&\frac{\alpha \mathrm{e}^{-2\pi \mathrm{i}(f+f_c)r_t/c}}{\sqrt{4\pi r_t^2}}\\ &\times\sqrt{A_{\text{eff},r}(f+f_c;\theta_t,\varphi_t)},\end{aligned} \tag{8}$$

where α is a complex circularly symmetric Gaussian random variable with variance σ_{RCS} (modeling the target response, with σ_{RCS} being the radar cross-section of the target), and $A_{\text{eff},r}(f;\theta,\varphi) = \frac{(c/f)^2}{4\pi}G_{\text{rx,r}}(\theta,\varphi)$ is the effective area of the receive antenna. The received signal is $z_r(t;r_t,\theta_t,\varphi_t)+n_r(t)$ if a target is present, and $n_r(t)$ otherwise, where $z_r(t;r_t,\theta_t,\varphi_t)$ is the inverse Fourier transform of $Z_r(f;r_t,\theta_t,\varphi_t)$ and $n_r(t)$ is the complex additive white Gaussian noise with power spectral density (PSD) $\sigma_{n,r}^2$.

[4]This problem can also be solved using different methods. However, the focus of this manuscript is not on the algorithmic side but on showing that this RIS-based architecture can be competitive with fully digital MIMO systems, and what is key here is that (7) and the corresponding problem for the MIMO system are solved with the same technique.

After standard matched-filtering, the SNR at the radar receiver, conditioned on the symbol a, when a target is present at (r_t,θ_t,φ_t) is:[5]

$$\begin{aligned}\text{SNR}_r(a,\theta_t,\varphi_t) &= \frac{\mathbb{E}\big[\|z_t(t;r_t,\theta_t,\varphi_t)\|^2 \mid a\big]}{\sigma_{n,r}^2}\\ &= \frac{\mathbb{E}\big[\|Z_t(f;r_t,\theta_t,\varphi_t)\|^2 \mid a\big]}{\sigma_{n,r}^2}\\ &= \frac{a\sigma_{\text{RCS}}G_{\text{rx,r}}(\theta_t,\varphi_t)T}{(4\pi)^3 r_t^4\sigma_{n,r}^2}\int_{\mathbb{R}}\left(\frac{B(f;r_t,\theta_t,\varphi_t)}{(f+f_c)/c}\right)^2 df,\end{aligned} \tag{9}$$

where we have used Parseval's theorem and Eqs. (3) and (6). Since the target response has been modeled as a complex circularly symmetric Gaussian random variable (namely, a Swerling 1 target fluctuation), the probability of detection of the likelihood ratio receiver for a given probability of false alarm (P_{fa}) is equal to[6]

$$P_{\text{d}}(a,\theta_t,\varphi_t) = P_{\text{fa}}^{1/(1+\text{SNR}_r(a,\theta_t,\varphi_t))}. \tag{10}$$

Given the radar beam is steered through successive pointing directions (typically half a beamwidth apart, mimicking mechanical scanning), the angular position (θ_t,φ_t) of a potential target can be considered a random vector uniformly distributed within half the beamwidth of the desired radar beam. The symbol a follows the probability distribution used for communication. The average detection probability is thus:

$$P_{\text{d}} = \mathbb{E}\left[P_{\text{fa}}^{1/(1+\text{SNR}_r(a,\theta_t,\varphi_t))}\right]. \tag{11}$$

For data communication, the transmitter has perfect CSI, and performance is measured by the data transmission rate. Assuming line-of-sight free-space propagation, the Fourier transform of the complex envelope of the signal received by the communication user at (r_u,θ_u,φ_u) is:

$$Z_u(f;r_u,\theta_u,\varphi_u) = Y(f;r_u,\theta_u,\varphi_u)\sqrt{A_{\text{eff},u}(f+f_c)}, \tag{12}$$

where $A_{\text{eff},u}(f) = \frac{(c/f)^2}{4\pi}G_{\text{rx},u}$ is the effective area of the receive antenna, with $G_{\text{rx},u}$ being the antenna gain. Therefore, the signal received is $z_u(t;r_u,\theta_u,\varphi_u)+n_u(t)$, where $z_u(t;r_u,\theta_u,\varphi_u)$ is the inverse Fourier transform of $Z_u(f;r_u,\theta_u,\varphi_u)$, and $n_u(t)$ is the complex additive white Gaussian noise with PSD $\sigma_{n,u}^2$.

Using Eqs. (3) and (6), the SNR at the communication user located at at (r_u,θ_u,φ_u) is:[7]

$$\begin{aligned}\text{SNR}_u(\theta_u,\varphi_u) &= \frac{\mathbb{E}\big[\|z_u(t;r_u,\theta_u,\varphi_u)\|^2\big]}{\sigma_{n,u}^2}\\ &= \frac{\mathbb{E}\big[\|Z_u(f;r_u,\theta_u,\varphi_u)\|^2\big]}{\sigma_{n,u}^2}\end{aligned}$$

[5]If $g:\mathbb{R}\to\mathbb{C}$ is a square-integral complex function, $\|g(t)\|$ is defined as $\|g(t)\| = (\int_{\mathbb{R}}|g(t)|^2dt)^{1/2}$.

[6]For N_p coherently integrated pulses, the SNR in (9) increases by N_p, and the probability of detection in (10) is updated accordingly.

[7]Recall that $\mathbb{E}[|a|^2]=1$.

$$= \frac{G_{\text{rx,u}} T}{(4\pi r_u)^2 \sigma_{n,u}^2} \int_{\mathbb{R}} \left(\frac{B(f; r_u, \theta_u, \varphi_u)}{(f + f_c)/c} \right)^2 df, \quad (13)$$

and the data transmission rate is:[8]

$$R(\theta_u, \varphi_u) = \log_2\big(1 + \text{SNR}_u(r_u, \theta_u, \varphi_u)\big) \quad (14)$$

bits per channel use. Since user position can vary during data packet transmission, the SNR may change. Here, we assume the user's direction (θ_u, φ_u) is uniformly distributed within half the beam dedicated to communication.[9] The average rate is:

$$R = \mathbb{E}\left[\log_2\big(1 + \text{SNR}_u(\theta_u, \varphi_u)\big)\right] \quad (15)$$

bits per channel use.

IV. Numerical results

We consider a 10×10 transmitting RIS, comprising $M = 100$ elements, illuminated by $J = 4$ sources. Both the RIS elements and the sources are modeled with a cosine power beampattern. The channel coefficient $G_{ij}(f; \theta, \varphi)$, representing the coupling between the i-th RIS element and the j-th source, is modeled as the product of the term accounting for the free-space propagation, the amplitude beampattern of the j-th source towards the i-th RIS element, and the effective area of the i-th RIS element towards the j-th source. The symbol a follows a complex circularly Gaussian distribution, the duration of the pulse $s_j(t)$ is $T = 0.64\,\mu\text{s}$, the bandwidth is $W = 100\,\text{MHz}$, and the carrier frequency is $f_c = 3\,\text{GHz}$. The RIS elements are spaced half a wavelength apart, and the four sources are positioned $60\,\text{cm}$ from the RIS, each corresponding to one of its four quadrants. For numerical evaluation, we use $K = 64$ uniformly spaced frequency sampling points within $[-50\,\text{MHz}, 50\,\text{MHz}]$, and 36×36 uniformly spaced angular sampling points within $[-90°, 90°] \times [-90°, 90°]$, totaling $L = 1296$ spatial points.

The desired beampattern consists of two beams: one for radar operation, with a height of $(1024\eta/(W \sin\frac{\pi}{8}))^{1/2}$ for the frequency band $[-W/2, -W/4]$ and the angular region $(\theta, \varphi) \in [0, \pi/8]^2$, and another for communication, with a height of $(256(1-\eta)/(W\sqrt{2} - W\sin\frac{\pi}{8}))^{1/2}$ across the entire available band $[-W/2, W/2]$ and the angular region $(\theta, \varphi) \in [-\pi/4, -\pi/8]^2$. Here, $\eta \in [0, 1]$ is a parameter controlling the power allocation between the two functionalities: the power dedicated to radar and communication is $8\eta\,\text{W}$ and $8(1-\eta)\,\text{W}$, respectively, summing to a total radiated power of $8\,\text{W}$ for the desired beampattern. The available power for solving the beampattern matching problem in (7) is $P = 10\,\text{W}$, the number of signal samples is $N = \lfloor WT \rfloor = 64$, and the weights $w_{k\ell}$ are unity for all frequency and angular sampling points.

[8]The quantity in (14) is the capacity of a Gaussian channel; it represents the supremum of the achievable rates and can be approached by using Gaussian symbols.

[9]Real-time solution of Problem (7) might be too computationally intensive. The DFRC transmitter may update beampatterns (one for each radar scanning direction) only when the user's angular position changes significantly.

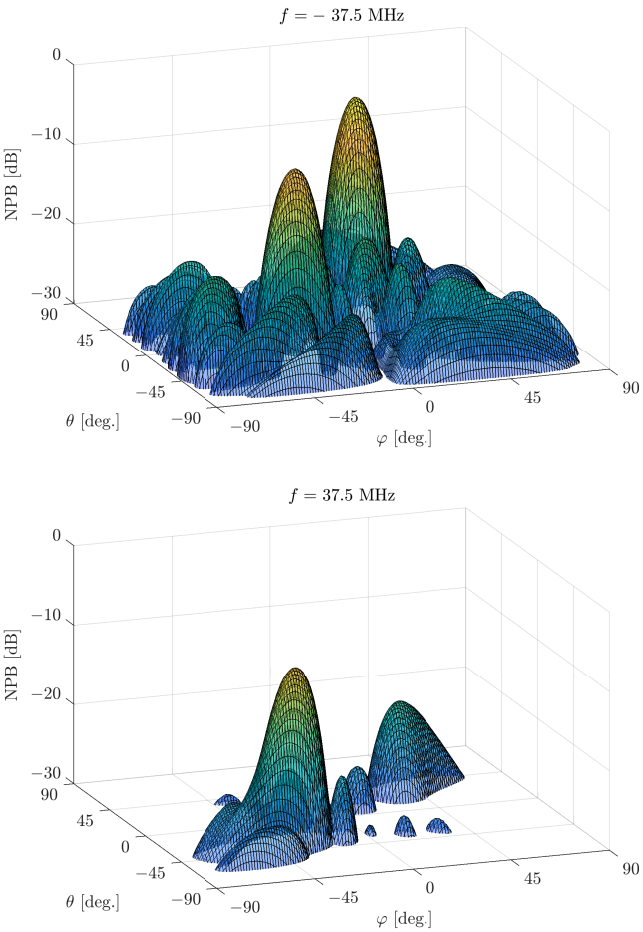

Figure 2. Normalized power beampattern (synthesized with the RIS-based DFRC system) as a function of elevation and azimuth for two frequency cuts when $\eta = 0.5$.

Fig. 2 illustrates the normalized power beampattern (NPB) —defined as $B^2(f; \theta, \varphi)$ normalized by its maximum value— achieved with the RIS-based DFRC architecture for $\eta = 0.5$, representing an equal power split in the desired beampattern between radar and communication. The NPB is plotted as a function of azimuth and elevation for two specific frequency slices. The figure demonstrates that the two beams at $f = -37.5\,\text{MHz}$ (where both functions are active) and the single beam at $f = 37.5\,\text{MHz}$ (where only communication is active) are well-formed, with relatively low sidelobe levels.

Fig. 3 presents the probability of detection (for $P_{\text{fa}} = 10^{-6}$) plotted against the data transmission rate. The curve is obtained by varying η (the power split between the desired beampattern) and plotting the corresponding (R, P_{d}) pair. This plot serves as a *system operating characteristic*, revealing the fundamental tradeoff between radar and communication functionalities and the achievable operating points. For comparison, we also consider a 10×10 fully digital MIMO system and evaluate the performance across different SNR regimes.

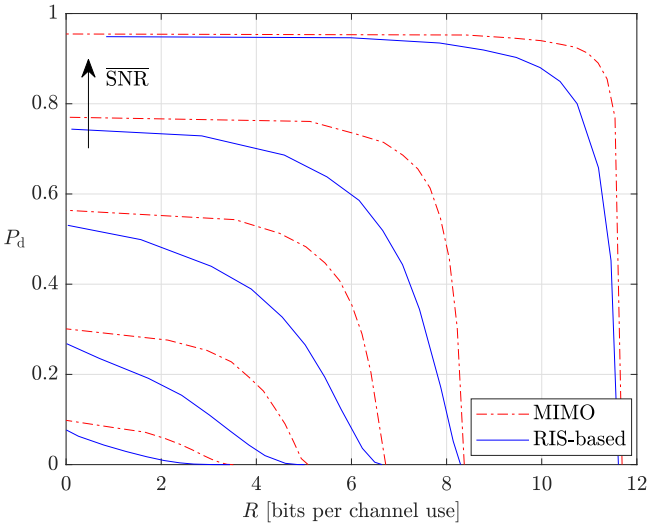

Figure 3. Average detection probability vs the average data transmission rate for the RIS-based and MIMO DFRC systems and for different values of the nominal SNR at the user and radar sides ($\overline{\rm SNR} = 5, 10, 15, 20, 30$ dB).

To this end, let $\overline{\rm SNR}_t$ and $\overline{\rm SNR}_u$ be the *nominal* SNRs at the radar and user receivers, respectively, obtained when the desired beampattern is used with all power dedicated to either radar ($\eta = 1$ for $\overline{\rm SNR}_t$) or communication ($\eta = 0$ for $\overline{\rm SNR}_u$), with the target and user at the center of the corresponding beam. In our analysis, we set $\overline{\rm SNR}_t = \overline{\rm SNR}_u = \overline{\rm SNR}$ and examine performance for $\overline{\rm SNR} = 5, 10, 15, 20, 30\,{\rm dB}$. The figure illustrates the inherent tradeoff between the radar and communication functions and the accessible operating region for the system designer. It is observed that the MIMO DFRC system outperforms the RIS-based system, thanks to its higher degrees of freedom. However, this performance advantage comes at the cost of significantly higher hardware complexity and expense, as the MIMO system employs 100 active elements compared to the RIS-based system's 4.

V. Conclusion

This work has effectively demonstrated the significant potential of a RIS-based transmit architecture for ISAC systems. By jointly designing the source waveforms and RIS phases, we achieved effective beampattern control, enabling the simultaneous generation of beams optimized for both radar and communication. Our analysis underscores the inherent tradeoff between the performance of these two functionalities, as illustrated by a system operating characteristic revealing the achievable $(R, P_{\rm d})$ pairs. Notably, even with the use of significantly fewer active sources compared to fully digital MIMO systems, the RIS-based architecture exhibits promising performance in terms of achievable data transmission rate and detection probability.

References

[1] A. Hassanien, M. Amin, Y. Zhang, and F. Ahmad, "Dual-function radar-communications: Information embedding using sidelobe control and waveform diversity," *IEEE Trans. Signal Process.*, vol. 64, no. 8, pp. 2168–2181, 2016.

[2] J. Johnston, L. Venturino, E. Grossi, M. Lops, and X. Wang, "MIMO OFDM dual-function radar-communication under error rate and beampattern constraints," *IEEE J. Sel. Topics Signal Process.*, vol. 40, no. 6, pp. 1951–1964, 2022.

[3] F. Liu, Y. Cui, C. Masouros, J. Xu, T. X. Han, Y. C. Eldar, and S. Buzzi, "Integrated sensing and communications: Toward dual-functional wireless networks for 6G and beyond," *IEEE J. Sel. Topics Signal Process.*, vol. 40, no. 6, pp. 1728–1767, 2022.

[4] X. Gao, L. Dai, and A. M. Sayeed, "Low RF-complexity technologies to enable millimeter-wave MIMO with large antenna array for 5G wireless communications," *IEEE Commun. Mag.*, vol. 56, no. 4, pp. 211–217, 2018.

[5] A. F. Molisch, V. V. Ratnam, S. Han, Z. Li, S. L. H. Nguyen, L. Li, and K. Haneda, "Hybrid beamforming for massive MIMO: A survey," *IEEE Commun. Mag.*, vol. 55, no. 9, pp. 134–141, 2017.

[6] V. Jamali, A. M. Tulino, G. Fischer, R. R. Müller, and R. Schober, "Intelligent surface-aided transmitter architectures for millimeter-wave ultra massive MIMO systems," *IEEE Open J. Commun. Soc.*, vol. 2, pp. 144–167, 2021.

[7] M. Di Renzo, A. Zappone, M. Debbah, M.-S. Alouini, C. Yuen, J. de Rosny, and S. Tretyakov, "Smart radio environments empowered by reconfigurable intelligent surfaces: How it works, state of research, and the road ahead," *IEEE J. Sel. Areas Commun.*, vol. 38, no. 11, pp. 2450–2525, 2020.

[8] E. Basar and H. V. Poor, "Present and future of reconfigurable intelligent surface-empowered communications [perspectives]," *IEEE Signal Process. Mag.*, vol. 38, no. 6, pp. 146–152, 2021.

[9] Q. Li, M. Wen, and M. Di Renzo, "Single-RF MIMO: From spatial modulation to metasurface-based modulation," *IEEE Trans. Wireless Commun.*, vol. 28, no. 4, pp. 88–95, 2021.

[10] S. Buzzi, E. Grossi, M. Lops, and L. Venturino, "Radar target detection aided by reconfigurable intelligent surfaces," *IEEE Signal Process. Lett.*, vol. 28, pp. 1315–1319, 2021.

[11] A. Aubry, A. De Maio, and M. Rosamilia, "Reconfigurable intelligent surfaces for N-LOS radar surveillance," *IEEE Trans. Veh. Technol.*, vol. 70, no. 10, pp. 10 735–10 749, 2021.

[12] S. Buzzi, E. Grossi, M. Lops, and L. Venturino, "Foundations of MIMO radar detection aided by reconfigurable intelligent surfaces," *IEEE Trans. Signal Process.*, vol. 70, pp. 1749–1763, 2022.

[13] M. Rihan, E. Grossi, L. Venturino, and S. Buzzi, "Spatial diversity in radar detection via active reconfigurable intelligent surfaces," *IEEE Signal Process. Lett.*, vol. 29, pp. 1242–1246, 2022.

[14] S. Gao, X. Cheng, and L. Yang, "Spatial multiplexing with limited RF chains: Generalized beamspace modulation (GBM) for mmWave massive MIMO," *IEEE J. Sel. Areas Commun.*, vol. 37, no. 9, pp. 2029–2039, 2019.

[15] J. Wang, L. He, and J. Song, "Towards higher spectral efficiency: Spatial path index modulation improves Millimeter-Wave hybrid beamforming," *IEEE J. Sel. Topics Signal Process.*, vol. 13, no. 6, pp. 1348–1359, 2019.

[16] R. Liu, M. Li, H. Luo, Q. Liu, and A. L. Swindlehurst, "Integrated sensing and communication with reconfigurable intelligent surfaces: Opportunities, applications, and future directions," *IEEE Wireless Commun.*, vol. 30, no. 1, pp. 50–57, 2023.

[17] Z. Esmaeilbeig, A. Eamaz, K. V. Mishra, and M. Soltanalian, "Quantized phase-shift design of active IRS for integrated sensing and communications," in *IEEE Int. Conf. Acoustics, Speech, and Signal Process. Workshops (ICASSPW)*, 2023.

[18] P. Stoica, J. Li, and Y. Xie, "On probing signal design for MIMO radar," *IEEE Trans. Signal Process.*, vol. 55, no. 8, pp. 4151–4161, 2007.

[19] D. R. Fuhrmann and G. San Antonio, "Transmit beamforming for MIMO radar systems using signal cross-correlation," *IEEE Trans. Aerosp. Electron. Syst.*, vol. 44, no. 1, pp. 171–186, 2008.

[20] S. Ahmed and M.-S. Alouini, "MIMO radar transmit beampattern design without synthesising the covariance matrix," *IEEE Trans. Signal Process.*, vol. 62, no. 9, pp. 2278–2289, 2014.

[21] H. He, P. Stoica, and J. Li, "Wideband MIMO systems: Signal design for transmit beampattern synthesis," *IEEE Trans. Signal Process.*, vol. 59, no. 2, pp. 618–628, Feb. 2011.

[22] K. Alhujaili, V. Monga, and M. Rangaswamy, "Transmit MIMO radar beampattern design via optimization on the complex circle manifold," *IEEE Trans. Signal Process.*, vol. 67, no. 13, pp. 3561–3575, 2019.

[23] X. Liu, T. Huang, N. Shlezinger, Y. Liu, J. Zhou, and Y. C. Eldar, "Joint transmit beamforming for multiuser MIMO communications and MIMO radar," *IEEE Trans. Signal Process.*, vol. 68, 2020.

[24] X. Wang, Z. Fei, Z. Zheng, and J. Guo, "Joint waveform design and passive beamforming for RIS-assisted dual-functional radar-communication system," *IEEE Trans. Veh. Technol.*, vol. 70, no. 5, pp. 5131–5136, 2021.

[25] H. Luo, R. Liu, M. Li, Y. Liu, and Q. Liu, "Joint beamforming design for RIS-assisted integrated sensing and communication systems," *IEEE Trans. Veh. Technol.*, vol. 71, no. 12, pp. 13 393–13 397, 2022.

[26] M. Rahal, B. Denis, K. Keykhosravi, M. F. Keskin, B. Uguen, G. C. Alexandropoulos, and H. Wymeersch, "Arbitrary beam pattern approximation via RISs with measured element responses," in *Joint Europ. Conf. Netw. Commun. & 6G Summit (EuCNC/6G Summit)*, 2022.

[27] R. Xiong, K. Yine, T. Mi, J. Lu, K. Wan, and R. Qiu, "Fair beam allocations through reconfigurable intelligent surfaces," *IEEE J. Sel. Areas Commun.*, vol. 42, no. 11, pp. 3095–3109, 2024.

[28] E. Grossi and L. Venturino, "Beampattern design for radars with reconfigurable intelligent surfaces," in *IEEE Radar Conf. (RadarConf)*, 2023.